Available online at www.sciencedirect.com
SCIENCE DIRECT®
Polymer 44 (2003) 7459–7465
polymer
www.elsevier.com/locate/polymer

Kinetics of phase separation and crystallization in poly(ethylene-ran-hexene) and poly(ethylene-ran-octene)

Go Matsuba*,[1], Katsumi Shimizu[2], Howard Wang[3], Zhigang Wang[4], Charles C. Han[5]

Polymers Division, National Institute of Standards and Technology, 100 Bureau Drive MS 8543, Gaithersburg, MD 20899-8543, USA

Received 11 June 2003; received in revised form 16 September 2003; accepted 18 September 2003

Abstract

The kinetics of phase separation and crystallization in the blends of poly(ethylene-ran-hexene) (PEH) and poly(ethylene-ran-octene) (PEOC) at several compositions were studied using phase contrast optical microscopy and time-resolved simultaneous small-angle X-ray scattering and wide-angle X-ray diffraction. The phase contrast optical microscopy showed the interconnected bicontinuous structure during phase separation process, which is characteristic of a spinodal decomposition. During isothermal crystallization, the average lamellar spacing increases with time for blends at all concentrations. The crystallinity and crystal growth rate depend on the PEH concentration. At dilute PEH concentrations, crystallization of PEH chains is difficult because they are surrounded by many non-crystallizable PEOC chains. On the other hand, at higher PEH concentrations, crystallization processes are similar to pure PEH. For example, the spherulitic growth rates are similar for a PEH/PEOC = 50/50 blend and pure PEH.
Published by Elsevier Ltd.

Keywords: Phase separation; Phase diagram; Crystallization; Polyolefins; Blends

1. Introduction

In the plastic industry, olefin polymers are the most widely used materials. Blending with other polymers, such as elastomers and crystalline polymers, is a very easy and effective way to improve their mechanical and thermal properties. To understand the fundamental physics of blending these polymers is a very significance for control of specific compounding and manufacturing processes. In the case of linear low-density polyethylene blends, the mixtures can undergo both liquid–liquid phase separation (LLPS) and crystallization. These processes affect greatly the blend morphology and properties of the final products. Much attention has been directed toward determining and understanding correlation between LLPS and crystallization of several kinds of polyolefin blends with various microstructures [1–3]. Recent development in constrained geometry metallocene catalyst technology allows production of copolymers of α-olefins with both narrow molecular mass distribution and homogeneous comonomer distribution. These features make the new copolymers excellent for fundamental studies of structure property relationships of ethylene copolymers blended with other semicrystalline polymers.

Our group has paid much attention to the blends of poly(ethylene-ran-hexene) (PEH) and poly(ethylene-ran-butene) (PEB) [4–8] using differential scanning calorimetry (DSC), light scattering (LS) and optical microscopy (OM) methods. The PEH/PEB blends exhibit an upper critical solution temperature (UCST) at $T_{cri} = 146\,^{\circ}C$ and $\phi_{cri} = 0.44$ in the melt [4,5,8]. In the two-phase region above T_m, the corresponding morphology is bicontinuous and interconnected tubes, which are characteristic of the late stage of spinodal decomposition. By comparing of the rates between

* Corresponding author. Tel.: +81-774383143; fax: +81 774383146.
E-mail addresses: gm@pmsci.kuicr.kyoto-u.ac.jp (G. Matsuba), c.c.han@iccas.ac.cn (C.C. Han), charles.han@nist.gov (C.C. Han).
[1] Present address: Institute for Chemical Research, Kyoto University, Gokasho, Uji, Kyoto-fu 611-0011, Japan.
[2] Present address: High-throughput Factory, Harima Institute, RIKEN, Hyogo 679-5418, Japan.
[3] Present address: Department of Materials Science and Engineering, Michigan Technological University, Houghton, MI 49931, USA.
[4] Present address: Avary Dennison Corporation, Pasadena, CA 91103, USA.
[5] Present address: Joint Laboratory of Polymer Science and Materials, Institute of Chemistry, Chinese Academy of Sciences, Beijing, 100080, People's Republic of China. Tel.: +1-301-975-6772; fax: +1-301-975-4977.

0032-3861/$ - see front matter Published by Elsevier Ltd.
doi:10.1016/j.polymer.2003.09.032

LLPS and crystallization, we argued that the kinetic crossover from LLPS dominant to crystallization dominant is inevitable in a blend for which the critical temperature of the LLPS is well above the melting temperature of the blend.

In this study, we focus on the kinetics of LLPS and crystallization in the blend of PEH and poly(ethylene-ran-octene) (PEOC). The PEOC in particular has been shown to provide a higher toughening contribution than either poly(ethylene-ran-propylene) or PEB [9]. In recent years, many reports have been published about rheological property and crystalline morphology of PEOC [9–15], the properties of the blends of PEOC with high-density polyethylene [16], with isotactic polypropylene [17] and with polypropylene/ethylene-propylene rubber [16]. We carried out time-resolved simultaneous small-angle X-ray scattering (SAXS) and wide-angle X-ray diffraction (WAXD) and OM measurements at several temperatures. We discuss about PEH concentration dependence of LLPS and crystallization (especially nucleation) processes based on the dynamics of spinodal decomposition and Avrami nucleation kinetics.

2. Experimental

The statistical copolymers of PEH and PEOC were synthesized by the metallocene-catalysis. The PEH with weight-average molecular masses (M_w) of 112,000 and molecular polydispersity, $M_w/M_n \sim 2$, where M_n is number-average molecular masses, was supplied by ExxonMobil and PEOC with M_w of 153,000, $M_w/M_n \sim 2$, supplied by Dow Chemical [18]. The side chain densities of PEH and PEOC are 1:57 and 1:15 backbone carbons of hexene and octene, respectively [12]. The melting temperatures of PEH and PEOC were 120 and 50 °C, respectively, and were defined as endothermic peak temperatures at a heating rate of 10 °C/min using DSC. PEH is the only crystallizable component of this system above 60 °C. The blends of PEH and PEOC, which have the PEH mass fraction of 100% (PEH), 70% (H-70), 50% (H-50) and 30% (H-30), were prepared with the co-precipitation method. The blends were first dissolved in a hot xylene solution at 120 °C, and then the solution was cooled to 100 °C and kept for 24 h. The solution was then poured into methanol to precipitate the blends. After filtering, the obtained blends were washed with clean methanol and dried in a vacuum oven for 72 h before use. The mixtures were hot-pressed at (200 ± 2) °C to form films of 20 μm (for OM) or 1 mm (for SAXS and WAXD) and then quenched to room temperature.

The DSC measurements were carried out following the standard practice. Samples of 6–10 mg by mass were placed in sample pans and then into a Perkin–Elmer DSC 7 system under a helium atmosphere to prevent oxidation or degradation. The samples were heated from room temperature to 200 °C with heating rate of 10 °C/min. The effect of thermal conductivity is minimal. The melting temperature, T_m, were defined as the endothermic peak temperature at this heating rate, because the peak value is a better representation of the thermodynamic value and less susceptible to both the instrument resolution and kinetic issues. The OM measurements were carried out using a Leitz Wetzlar optical microscope with a Sony CCD camera (XC-77). A hot stage was used to control the sample temperature. The samples were melted at (200 ± 1.0) °C for 10 min and then quenched to the annealing temperatures between (130 ± 0.5) and (180 ± 0.5) °C for measurements. Time-resolved simultaneous SAXS/WAXD measurements were performed at Advanced Polymers Beamline (X27C) in the National Synchrotron Light Source (NSLS), Brookhaven National Laboratory (BNL). The storage ring was operated at an energy level of 2.8 GeV with a ring current 250 mA. The wavelength of X-ray beam was 1.366 Å with a beam size about 0.3–0.4 mm in diameter at the sample position. Synchrotron X-ray was collimated with three 2° tapered tantalum pinhole collimators. The SAXS/WAXD profiles were collected by position sensitive detectors (from European Molecular Biological Laboratory) with sample to detector distance of 1925 mm for SAXS and 110 mm for WAXD, respectively. Isothermal crystallization measurements were carried out with dual-chamber temperature apparatus described by Hsiao et al. [19,20]. The sample was melted at 200 °C for 10 min and quenched to 113.8 °C and time-resolved SAXS/WAXD measurement was performed during the isothermal crystallization process with a data acquisition time of 30 s per scan.

3. Results and discussion

Fig. 1 shows phase contrast optical micrographs of the H-50 sample melted at 200 °C for 10 min and isothermally annealed at 150 °C for (a) 0, (b) 102, (c) 153, (d) 253, (e) 353 and (f) 753 min. The scale bar in Fig. 1(a) is 40 μm and is the same for all pictures. Phase separation in the originally homogenous sample in Fig. 1(a) can be observed after annealing for 100 min at 150 °C. This annealing condition is above the equilibrium melting temperature, $T_m^\circ \sim 142$ °C [21,22]. After 102 min, the bicontinuous structure grows in Fig. 1(b) and characteristic length increases with annealing time in Fig. 1(c)–(f). This bicontinuous structure signifies the typical spinodal decomposition of LLPS.

For a semi-quantitative determination of the phase boundary, PEH/PEOC blend samples of different composition were annealed for a constant time (24 h) on the hot stage with phase contrast microscopy. Fig. 2 represents the observed results, with squares denoting homogeneous single-phase melts and triangles denoting two-phase melts. For PEH/PEOC blends, the UCST is about 171 °C, because the H-50 sample after annealed at 172 °C is homogeneous, while that at 170 °C exhibits phase separation. The phase boundary curve in Fig. 2 has some uncertainty mainly from

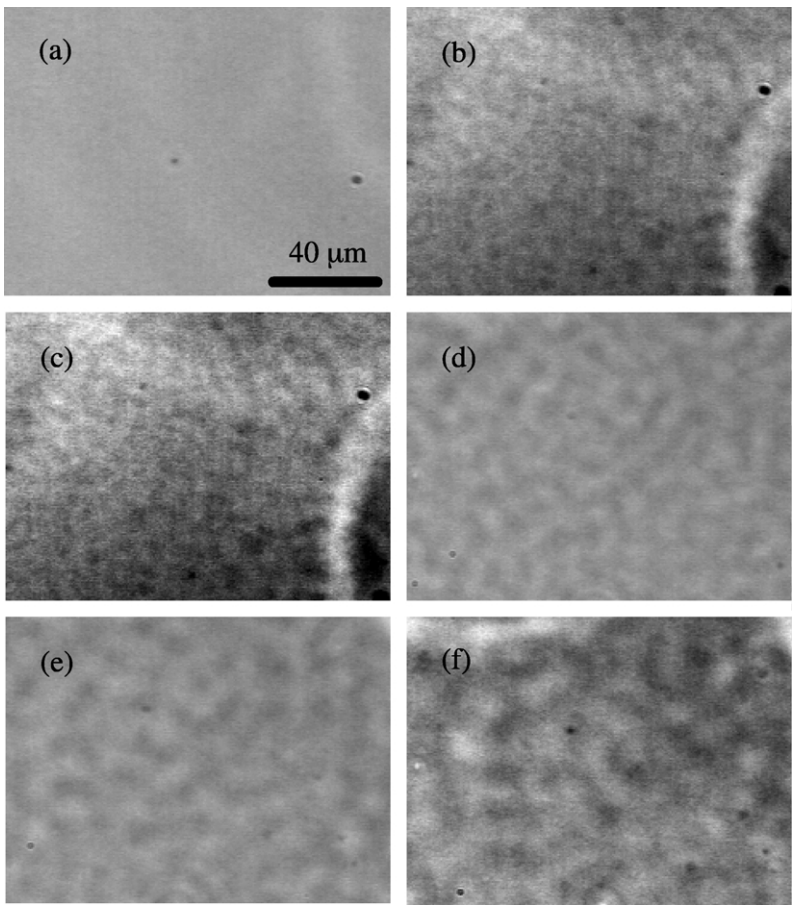

Fig. 1. Phase contrast optical micrographs of the H-50 blend annealing at 150 °C for (a) 0, (b) 102, (c) 153, (d) 253, (e) 353 and (f) 753 min. The scale bar in (a) is 40 μm and is the same for all.

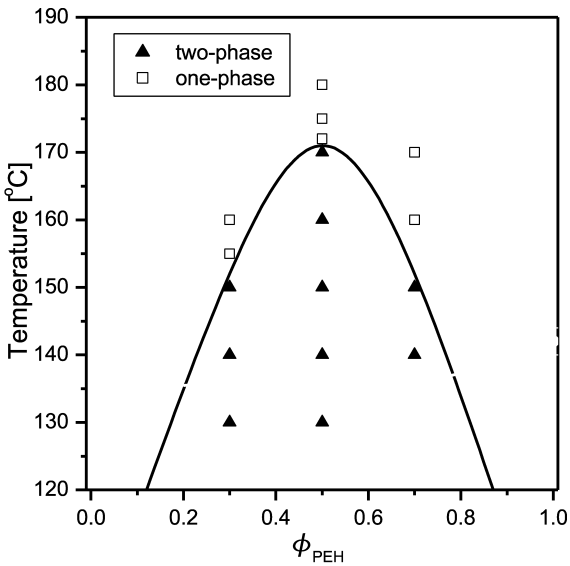

Fig. 2. Phase diagram of the PEH/PEOC blends. These lines are guides to the eye.

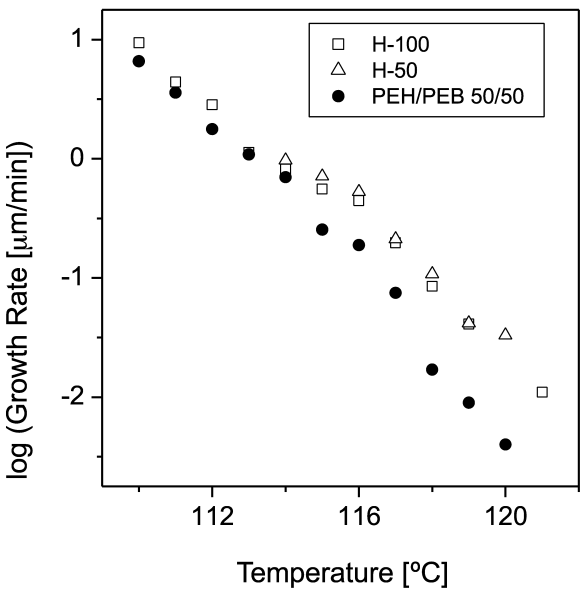

Fig. 3. The growth rate of average spherulite diameters at various isothermal crystallization temperatures for the H-50 (△) and H-100 (□) and PEH/PEB = 50:50 blend system (●).

the temperature controller (±0.5 °C). It is natural that the phase diagram determined by this method could depend on the annealing time due to the detection limit of our phase contrast microscope. On increasing with the annealing time, the phase boundary curve could increase slightly with temperature.

Fig. 3 shows the spherulitic growth rates of H-50, H-100 and PEH/PEB = 50:50 blend varied with quenching depth, $\delta T = T_m^\circ - T_c$, T_c being the isothermal crystallization temperature. These isothermal crystallization temperatures are just below the melting temperature of these polyethylene blends about 120 °C from the DSC measurement of each sample. The spherulite growth rate of H-50 is the same as that of H-100 as shown in Fig. 3. On the other hand, under small undercooling, the PEH/PEB blend with the same composition (PEH/PEB = 50:50), crystallized much slower than that in the PEH at elevated temperatures. By controlling the quenching condition of PEH/PEB blends, the growth kinetics of simultaneous ordering processes shows a crossover from crystallization dominated to phase separation dominated behavior [5–8]. In this study, we approximated the growth rate of liquid phases, l', when the viscosity of two components are similar and the temperature range of interest is small and well above the glass transition temperature ($T_g \sim -40$ °C), as below;

$$l' \propto T_{cri}/T - T_{cri}.$$

The detail derivation of this equation was described in our previous paper [5]. In the shallow quenching, the rate of spherulitic growth is slower than that of phase separation and the LLPS dominates. Crystals can grow fast by taking in the short polyethylene segments and through the phase separation medium while expelling the non-crystallizable chains, resulting in a spherulitic growth dominated morphology. However, in the deeper quenching, the rate of crystallization is much faster than that of phase separation and then more PEH chain segments become non-crystallizable. Annealing at 143 °C, the phase separation rate is about 0.02 μm/min from the phase contrast microscopy. We can estimate that the phase separation rate is 0.03–0.04 μm/min within 120–110 °C. The phase separation rate is smaller than the spherulite growth rate from Fig. 3. As a result, on crystallization of PEH/PEOC blends, the correlation between spherulite growth and LLPS processes are very similar to the deeper quenching of PEH/PEB blends.

Fig. 4(a) shows the typical time-resolved Lorentz-corrected SAXS intensity profiles (Iq^2) versus scattering vector q (= $4\pi \sin\theta/\lambda$, 2θ and λ being the scattering angle and the wavelength of X-ray, respectively) for H-70 during isothermal crystallization at 113.8 °C. Fig. 4(b) shows the corresponding WAXD intensity profiles. The initial SAXS profiles show a completely disordered structure in the undercooled melt. The scattered intensity profile exhibits a small maximum at about $q = 0.02$ Å^{-1} for 10 min, which subsequently increases until reaching a plateau value. The initial isothermal WAXD profiles show only one amorphous

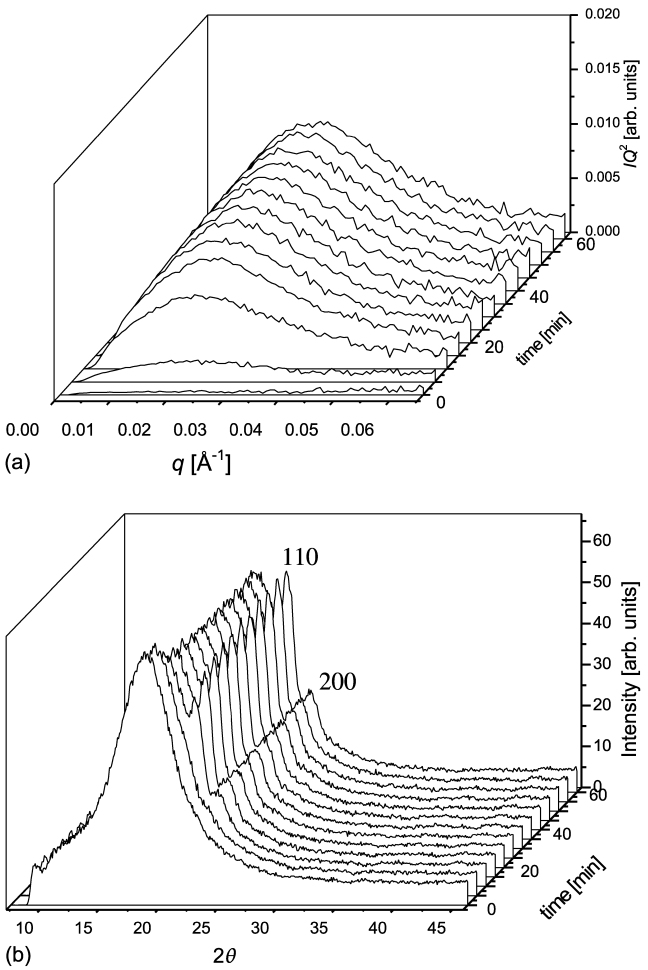

Fig. 4. (a) The time-resolved Lorentz-corrected SAXS intensity profiles and (b) WAXD intensity profiles of H-70, developed during isothermal crystallization at 113.8 °C.

peak. The evolution of an orthorhombic unit cell structure of PEH crystal can be followed through the development of the corresponding (110) and (200) reflections marked in Fig. 4(b). The intensities of the crystal reflections (110) and (200) increase notably during early stage of crystallization and remain almost constant during the late stages of crystallization.

From the time-resolved SAXS profiles, the long period, L (= $2\pi/q_{max}$, according to the Bragg law, and q_{max} is the q value at the SAXS peak position) and the invariant, Iq^2 (= Q) can be obtained. Fig. 5(a) and (b) indicate time evolution of the long period L and the invariant Q for each sample, respectively. The long period increases with the isothermal crystallization time. For pure PEH and PEH/PEB blends samples [7,8], one could find such phenomena especially in crystallization condition just below T_m. Some researchers found such long period increasing of ultra high density polyethylene [23], LLDPE [7,8] and pure PEOC [15] by lamellar thickening which is related to surface melting and re-crystallization processes of isothermal crystallization just below T_m. Polymer meta-stable crystals

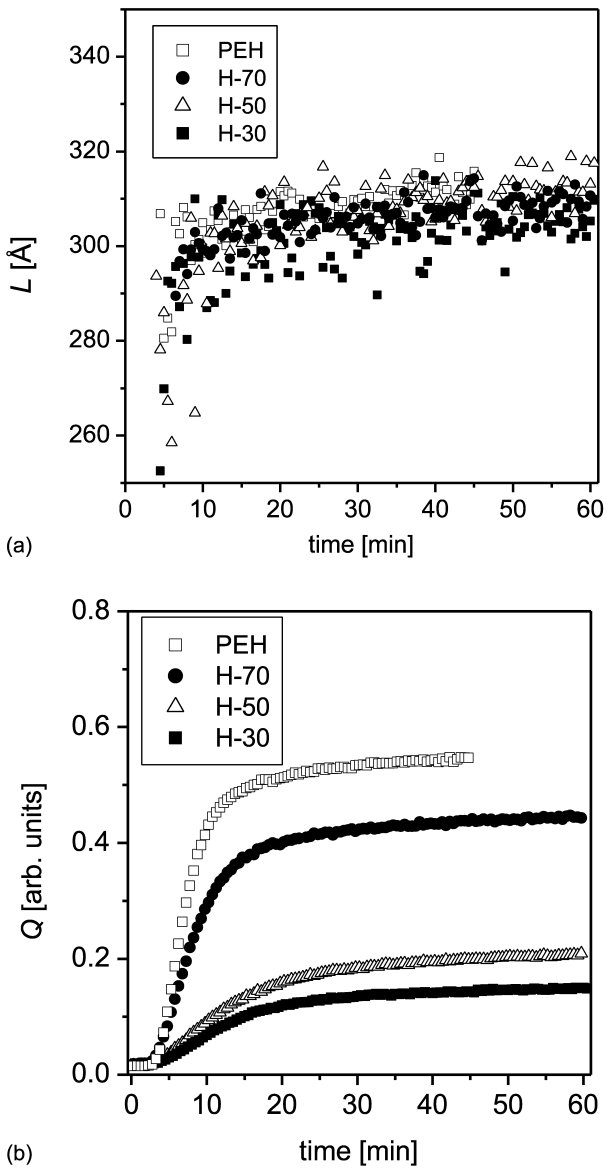

Fig. 5. (a) The long period, L, and (b) the invariant, Q, of lamella crystal versus isothermal crystallization time for H-100 (□), H-70 (●), H-50 (△) and H-30 (■).

have some defects especially during the early stage of crystallization. The meta-stable crystal could melt and re-crystallize involving complete refolding of polymer chains to eliminate defects because the segments are having enough mobility at higher isotherm temperatures to carry out this rearrangement. In this case, the lamellar long period is almost independent of PEOC concentration within error bars. Normally, the non-crystallizable chains can reside either at inter-lamella amorphous regions or at inter-lamella-stack regions. In the former, the lamellar long period would scale with PEOC concentration in the blend. In this study, however, the SAXS measurements indicate that PEOC chains reside not at the inter-lamella but mainly at the inter-lamella-stack region. This suggests the possibility of co-crystallization between PEH and PEOC. Our group showed that the PEH/PEB blends could co-crystallize from simultaneous small and wide angle X-ray scattering [8]. Such co-crystallization should affect the lamellar structures. The invariant Q indicates the density fluctuations. The value increases with time and PEH concentration because the PEH crystal grows and density fluctuations enhance with time.

For time-resolved WAXD profiles, the mass fraction of crystal (crystallinity, X_c) can be extracted [7,8]. Fig. 6 represent the time evolution of X_c at different PEH concentration annealing at 113.8 °C. Note that X_c in Fig. 6 has been normalized by the concentration of PEH component in the blends. The X_c's are about 13% for the PEH, 12% for the H-70, 9% for the H-50 and 8% for the H-30. The crystallinity depends on PEH concentration with a very special pattern.

Accordingly, the kinetics of crystallization is expressed as an Avrami-like curves [24,25]. The phenomenological Avrami equation can be written as

$$1 - X_c(t) = \exp(-kt^n)$$

where $X_c(t)$ is the fraction crystallized at time t by normalizing the $X_c(t) = 1$ at the long time limit of crystallization, k is a constant dependent on nucleation and growth rates and n is the Avrami exponent, related to the type of nucleation and growth geometry. We calculated Avrami exponents for PEH/PEOC blends listed in Table 1. It is interesting to notice that the normalized crystallinity and the Avrami exponent n depend on the PEH concentration at constant quenching depth δT. The Avrami exponents of PEH and H-70 are 3.5 and 3.0, respectively. This result suggests that the nucleation geometry is instantaneous sphere (three-dimensional system) and that some of the nuclei are born simultaneously while others are born sporadically, which is consistent with many reports about polyethylene crystallization [26]. However, the

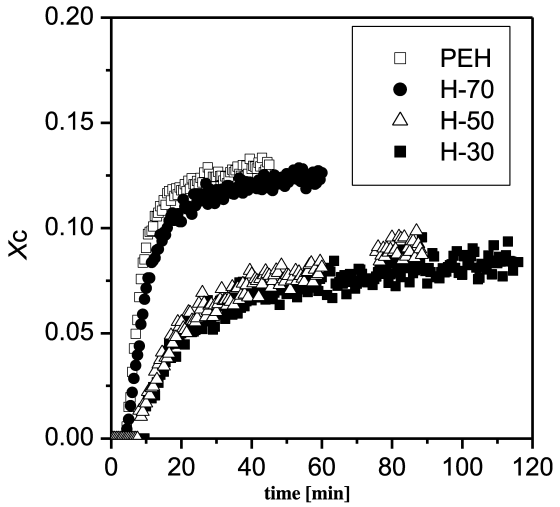

Fig. 6. The WAXD normalized crystallinity, X_c, versus isothermal crystallization time for H-100 (□), H-70 (●), H-50 (△) and H-30 (■). The relative standard deviations for X_c are less than 1%.

Table 1
Avrami exponent (n) for H-100, H-70, H-50 and H-30 at 113.8 °C

Sample	Avrami exponent (n)
H-100	3.5
H-70	3.0
H-50	1.8
H-30	1.5

Avrami exponent of H-50 and H-30 are 1.8 and 1.5, respectively, much smaller than that of H-100 or H-70. In similar system of PEH/PEB = 50/50, we have observed both fibril and isolated lamella crystal habits using atomic force microscopy [5]. Strobl et al. insisted that a crystallization process of branched polyethylene was dendritic growth due to decreasing the specific internal surface from their studies of small Avrami exponent [27,28]. However, in PEH/PEOC blends, the diffusion process of PEOC chain from the growth front is the dominant effect on decreasing the Avrami exponent. At dilute PEH concentrations, fewer PEH chains exist at the growth front of crystallization and the amorphous PEOC chains are expelled from the growth front of crystallization. The non-crystallizable PEOC chains surround the lamellar crystal and they prevent three-dimensional crystal growing. As a result, the Avrami exponent decreases with PEOC concentration.

Kelly and Cheng discussed the hierarchy of metastabilities for polymer blends and solutions in various temperature conditions [29,30]. When quenching a homogeneous blend into a regime of simultaneous phase separation and crystallization, the phase separation processes occur first because the system of two fluids is unstable thermodynamically and the phase separation growth does not require overcoming the energy barrier. In contrary, LLPS takes place and grows within a partially crystallized system since the isothermal crystallization temperature is sufficiently below T_m and then crystal structure and crystallization kinetics have some effects on LLPS. We have argued about the competition of two structure formation processes, crystallization (or spherulite growth) and late state phase coursing. In the dilute PEH concentration condition crystallized at 113.8 °C, crystallization rate becomes slower; crystallinity becomes lower as shown in Figs. 5(b) and 6. These results suggest that PEH chains become harder to crystallize for penetrating the longer 'PEH dilute region'. In particular, PEOC chains prevent PEH crystal from nucleating and growing. Such prevention by PEOC chain restricts the dimension of PEH nucleation and growth, and Avrami exponent ($n \sim 1.5$) decreases with increasing PEOC concentration. Metastable structure originated from phase separation has very quite effects on crystal structure [29,30]. We described that, in the system of such polyolefin blends, metastable system is a dominant states of all such transformation processes using time-resolved optical microscopy and scattering methods.

PEH concentration depends very much on Avrami exponent and crystallinity in Figs. 5–8 especially in PEH dilutes case. During the crystal growth, the phase separation processes continue and does not finish at all. That is to say, non-crystallizable PEOC chain diffusion process is the dominant in the nano scale structure different from the spherulite growth in micron scale structure.

Future studies will further explore the possibility of improving properties of LLDPE blends by changing the branching density, side chain length and molecular weights of LLDPE samples.

4. Conclusions

We have investigated the kinetics of LLPS and crystallization in the blends of PEH and PEOC. Several techniques, such as phase contrast optical microscopy, differential scanning calorimetry and time-resolved simultaneous SAXS and WAXD, are used to determine the phase separation boundary and understand the crystallization kinetics. The UCST of this PEH/PEOC blend is 171 °C. The phase separation pictures in the PEH/PEOC = 50:50 blend have shown the interconnected bicontinuous structures, characteristic of spinodal decomposition. The characteristic length increases with annealing time. The crystallinity and nucleation processes depend on the PEH concentration. At the dilute PEH concentrations, crystallinity and the Avrami exponent decreases with PEOC concentration because many non-crystallizable PEOC chains surround lamellar crystal. On the other hand, at the higher PEH concentrations, the crystallization processes are similar to pure PEH. For example, the spherulitic growth of PEH/PEOC = 50:50 sample is similar to that of pure PEH sample.

References

[1] Crist B, Hill MJ. J Polym Sci Part B: Polym Phys 1997;35(14):2329–53.
[2] Mandelkern L, Alamo RG, Wignall GD, Stehling EC. Trends Polym Sci 1996;4(11):377–83.
[3] Chen HY, Chum SP, Hiltner A, Baer E. Macromolecules 2001;34(12):4033–42.
[4] Wang H, Shimizu K, Hobbie EK, Wang ZG, Carson-Meredith J, Karim A, Amis EJ, Hsiao BS, Hsieh ET, Han CC. Macromolecules 2002;35(3):1072–8.
[5] Wang H, Shimizu K, Kim H, Hobbie EK, Wang ZG, Han CC. J Chem Phys 2002;116(16):7311–5.
[6] Shimizu K, Wang H, Wang ZG, Kim H, Han CC. Abstr Pap Am Chem S 2002;223:333.
[7] Wang H, Wang GZG, Han CC, Hsiao BS. Polym Mat Sci Engng Prep 2001;85:427–8.
[8] Han CC, Wang H, Shimizu K, Kim H, Hobbie EK, Wang ZG. Abstr Pap Am Chem S 2002;224:761.
[9] McNally T, McShane P, Nally GM, Murphy WR, Cook M, Miller A. Polymer 2002;43(13):3785–93.

[10] Chen HY, Chum SP, Hiltner A, Baer E. J Polym Sci Part B: Polym Phys 2001;39(14):1578–93.
[11] Alizadeh A, Richardson L, Xu J, McCartney S, Marand H, Cheung YW, Chum S. Macromolecules 1999;32(19):6221–35.
[12] Bensason S, Minick J, Moet A, Chum S, Hiltner A, Baer E. J Polym Sci Part B: Polym Phys 1996;34(7):1301–15.
[13] Bensason S, Stepanov EV, Chum S, Hiltner A, Baer E. Macromolecules 1997;30(8):2436–44.
[14] Tabtiang A, Parchana B, Venables RA, Inoue T. J Polym Sci Part B: Polym Phys 2001;39(3):380–9.
[15] Goderis B, Peeters M, Mathot VBF, Koch MHJ, Bras W, Ryan AJ, Reynaers H. J Polym Sci Part B: Polym Phys 2000;38(15):1975–91.
[16] Da Silva ALN, Rocha MCG, Coutinho FMB, Bretas RES, Scuracchio C. J Appl Polym Sci 2001;79(9):1634–9.
[17] Lee JH, Lee JK, Lee KH, Lee CH. Polymer J 2000;32(4):321–5.
[18] Certain equipment, instruments or materials are identified in the paper in order to adequately specify the experimental details. Such identification does not imply recommendation by the National Institute of Standards and Technology, nor does it imply the materials are necessarily the best available for the purpose.
[19] Hsiao BS, Chu B, Yeh F. July 1997 NSLS Newsletter; 1. http://nslsweb.nsls.bnl.gov/nsls/pubs/newsletters/pdfs/97-jul.pdf.
[20] Hsiao BS, Gardner KH, Wu DQ, Chu B. Polymer 1993;34(19):3996–4003.
[21] Kim MH, Phillips PJ, Lin JS. J Polym Sci Part B: Polym Phys 2000;38(1):154–70.
[22] Wagner J, Phillips PJ. Polymer 2001;42(21):8999–9013.
[23] Rastogi S, Spoelstra AB, Goossens JGP, Lemstra PJ. Macromolecules 1997;30(25):7880–9.
[24] Avrami M. J Chem Phys 1939;7:1103–12.
[25] Avrami M. J Chem Phys 1940;8:212–24.
[26] Schulz JM. Polymer crystallization: The development of crystalline order in thermoplastic polymers. New York: Oxford University Press; 2001. Chapters 5, 9, 10.
[27] Strobl GR, Engelke T, Maderek E, Urban G. Polymer 1983;24(12):1585–9.
[28] Maderek E, Strobl GR. Colloid Polym Sci 1983;261(6):471–6.
[29] Keller A, Cheng SZD. Polymer 1998;39(21):4461–87.
[30] Cheng SZD, Keller A. Annu Rev Mater Sci 1998;28(21):533–62.